



# Identified lung adenocarcinoma metabolic phenotypes and their association with tumor immune microenvironment

Xian-Ning Wu<sup>1</sup> · Dan Su<sup>2</sup> · Yi-De Mei<sup>3</sup> · Mei-Qing Xu<sup>1</sup> · Hao Zhang<sup>4</sup> · Ze-Yu Wang<sup>4</sup> · Li-Ling Li<sup>6,7</sup> · Li Peng<sup>8</sup> · Jun-Yi Jiang<sup>9</sup> · Jia-Yi Yang<sup>10</sup> · Dong-Jie Li<sup>11,12</sup> · Hui Cao<sup>13</sup> · Zhi-Wei Xia<sup>14</sup> · Wen-Jing Zeng<sup>16</sup> · Quan Cheng<sup>4,15,16</sup> · Nan Zhang<sup>5</sup>

Received: 1 August 2020 / Accepted: 18 February 2021 / Published online: 3 March 2021  
© The Author(s), under exclusive licence to Springer-Verlag GmbH, DE part of Springer Nature 2021

## Abstract

**Background** Lung adenocarcinoma (LUAD), a subtype of non-small cell lung cancer (NSCLC), causes high mortality around the world. Previous studies have suggested that the metabolic pattern of tumor is associated with tumor response to immunotherapy and patient's survival outcome. Yet, this relationship in LUAD is still unknown.

**Methods** Therefore, in this study, we identified the immune landscape in different tumor subtypes classified by metabolism-related genes expression with a large-scale dataset (tumor samples,  $n=2181$ ; normal samples,  $n=419$ ). We comprehensively correlated metabolism-related phenotypes with diverse clinicopathologic characteristics, genomic features, and immunotherapeutic efficacy in LUAD patients.

**Results** And we confirmed tumors with activated lipid metabolism tend to have higher immunocytes infiltration and better response to checkpoint immunotherapy. This work highlights the connection between the metabolic pattern of tumor and tumor immune infiltration in LUAD. A scoring system based on metabolism-related gene expression is not only able to predict prognosis of patient with LUAD but also applied to pan-cancer. LUAD response to checkpoint immunotherapy can also be predicted by this scoring system.

**Conclusions** This work revealed the significant connection between metabolic pattern of tumor and tumor immune infiltration, regulating LUAD patients' response to immunotherapy.

**Keywords** Lung adenocarcinoma · Metabolism · Immune infiltration · Immunotherapy · PD-1

## Abbreviations

AUC	Area under the curve
CNAs	Copy number alternations
DEGs	Differentially expressed genes
FDR	False discovery rate
FPKM	Fragments per kilobase million
GEO	Gene expression omnibus
GEP	Gene expression profile
GO	Gene ontology
GSVA	Gene set variation analysis
LUAD	Lung adenocarcinoma
LUSC	Lung squamous cell carcinoma
NSCLC	Non-small cell lung cancer

ROC	Receiver operating characteristic
TIDE	Tumor immune dysfunction and exclusion
TME	Tumor microenvironment
TPM	Transcripts per kilobase million
t-SNE	T-distributed stochastic neighbor embedding

## Introduction

Lung cancer is the leading cause of cancer incidence and high mortality globally. Non-small cell lung cancer (NSCLC) accounts for 85% of all lung cancer, and 5-year survival rate of patients with NSCLC is less than 20% [1]. NSCLC is further subdivided into lung adenocarcinoma (LUAD) and lung squamous cell carcinoma (LUSC) based on histologic features [2]. Although LUSC has demonstrated a positive correlation with smoking, its counterpart, LUAD, manifests a poor relationship with smoking and is usually discovered in non-smokers [1, 2].

✉ Quan Cheng  
chengquan@csu.edu.cn

✉ Nan Zhang  
awekevin@onethird-lab.com

Extended author information available on the last page of the article

Checkpoint blockade immunotherapy has achieved success in NSCLC treating [3, 4]. However, tumor sensitivity to immunotherapy varies and is limited by multiple factors.

Although normal cells chiefly depend on oxidative phosphorylation for ATP generation, tumor cells prefer glycolysis even with adequate oxygen, a phenomenon called the Warburg effect [5]. The accumulation of lactate, a product of glycolysis, in the extracellular matrix not only contributes to the acidic tumor microenvironment (TME), but also affects immunocytes infiltration. Previous studies reported that acidic TME could affect T cell-mediated immunity and impair immunocytes function [6]. Besides, an immune checkpoint can promote the cross talk between tumor cells and immunocytes [7]. Multiple metabolic-related pathways, such as the PI3K/AKT/mTOR pathway and the JAK/STAT pathway, have also been associated with immunotherapy resistance [8, 9]. Therefore, the metabolism of tumor cells affects TME and immune infiltration profile to alter immunotherapy efficiency.

Checkpoint blockade immunotherapy enhances T cell-mediated immunity by targeting immune regulators, including PD-1 and CTLA-4 [10]. This strategy suppresses tumor immune escape and promotes cytotoxic immunocytes to attack tumor cells [11, 12]. For example, a tumor with a lower infiltration ratio of CD8 + T cells, CH4 + T cells, NK cells and T regulatory cells exhibits worse response to checkpoint-based immunotherapy [12–14]. The role of immunocytes is highly related to tumor response to checkpoint blockade immunotherapy. Notably, previous research has reported a significant difference in immune infiltration landscape between various NSCLC subtypes [15]. Therefore, variation in immune infiltration may result in tumor resistance to checkpoint-based immunotherapy.

In this study, we collected 2752 metabolism-related genes and explored their expression profile in a large-scale dataset. Remarkably, based on metabolism-related gene expression in LUAD, we classified samples into two groups: Metcluster 1 and Metcluster 2. And these two groups are not only manifest with differences in immune profile but also able to predict patient's survival outcomes. The biofunction between the two groups supported the difference in the enrichment of metabolic pathways and immunity-related pathways. Preferential expression of the checkpoint, immune ligands and antigen-presenting cells were also identified between the two groups, indicating that metabolism-related genes can alter tumor response to checkpoint blockade immunotherapy by affecting immune infiltration profile. Moreover, different expression genes of the two groups were filtered and clustered to validate former results. As predicted, similar difference was observed and a scoring system was built to assist in the evaluation of the patient's survival outcome and tumor response to

immunotherapy. Generally, this study confirms the association of tumor metabolic and tumor immune infiltration profiles, which encourages future research.

## Materials and methods

### LUAD datasets and preprocessing

Publicly available LUAD gene expression datasets were searched in multiple data repositories. Ten cohorts of samples from patients with LUAD ( $n=2181$ ) were included in this study: GSE13213, GSE14814, GSE30219, GSE31210, GSE37745, GSE50081, GSE68465, GSE72094, GSE81089 and TCGA-LUAD. The microarray datasets were downloaded from the Gene Expression Omnibus (GEO; <https://www.ncbi.nlm.nih.gov/geo/>). The raw data from the microarray datasets were generated by Affymetrix and Agilent. The RMA algorithm in the Affy software package was subsequently applied to process the raw data from Affymetrix for quantile normalization and background correction. The raw data from Agilent were processed using the *limma* software package in R. The Cancer Genome Atlas (TCGA) datasets were downloaded from UCSC Xena (<https://xenabrowse.ucsc.edu/>). The normal tissue samples were downloaded from GTEx database (<http://commonfund.nih.gov/GTEx/>). The RNA-sequencing (RNA-seq) data were downloaded from the TCGA data portal. The fragments per kilobase million (FPKM) values were then transformed into transcripts per kilobase million (TPM) values. All data were analyzed with the R software (version 3.6.1) and R Bioconductor packages.

### Identification of LUAD subclasses

A published list of 2752 metabolism-relevant genes was achieved for subsequent clustering [16]. A filtering procedure was conducted. First, 1714 common candidate genes among the included cohorts were selected for t-distributed stochastic neighbor embedding (t-SNE). In total, 559 candidate metabolic genes with  $P < 0.05$  were finally selected for clustering. Subsequently, tumors with qualitatively diverse metabolic gene patterns were classified using *kmdist* [17], which identified metabolic-related patterns and grouped patients for further analysis. This method was also applied to the TCGA-LUAD cohort by using the same candidate genes. The optimal number of clusters and their stability and reliability in both the meta-cohort and TCGA cohort were determined using the ConsensusClusterPlus R package [18]. The t-SNE-based approach was then used to validate the subtype assignments using the mRNA expression data of the metabolic-related genes.

## Estimation of immune infiltration

Single-sample GSEA (ssGSEA) algorithm was used to quantify the proportion of the immune cell in the LUAD samples [19]. The gene sets include 782 genes for predicting the abundance of 28 TIICs in individual tissue samples (<http://software.broadinstitute.org/gsea/msigdb/index.jsp>). ssGSEA was applied since it could allow for sensitive and specific discrimination of 28 human infiltration immune cell phenotypes [20]. The following 28 types of immune cells were obtained: activated B cells (Ba), activated CD4 + T cells (CD4 + Ta), activated CD8 + T cells (CD8 + Ta), activated dendritic cells (DCa), CD56bright natural killer cells (CD56 + NK), CD56dim natural killer cells (CD56- NK), central memory CD4 + T cells (CD4 + Tcm), central memory CD8 + T cells (CD8 + Tcm), effector memory CD4 + T cells (CD4 + Tem), effector memory CD8 + T cells (CD8 + Tem), eosinophils, gamma delta T cells ( $\gamma\delta$ T), immature B cells (Bi), immature dendritic cells (DCi), mast cells, myeloid-derived suppressor cells (MDSC), memory B cells (Bm), monocytes, natural killer cells (NK), natural killer T cells (NK T), neutrophils, plasmacytoid dendritic cells (DCp), macrophages, regulatory T cells (Tregs), follicular helper T cells (Tfh), type-1 T helper cells (Th1), type-17 T helper cells (Th17) and type-2 T helper cells (Th2). The relative expression of the 28 TIICs in each sample was determined.

## Identification of metabolic-related differentially expressed genes (DEGs)

To identify genes associated with metabolic-related patterns, patients were grouped into two distinct metabolic clusters based on the diverse expression of metabolism-relevant genes. The *limma* package in *R* was used to determine DEGs associated with the two metabolic-related patterns [21]. Adjusted  $P < 0.01$  was set as the significance criteria used to determine the DEGs among the metabolic subtypes.

## Generation of metabolic gene signatures and dimension reduction

The DEGs among Metclusters were standardized in all the samples in the TCGA-LUAD cohort. Univariate Cox regression analysis was used to identify representative DEGs. An unsupervised clustering method [22] was used to classify patients into two gene clusters for further analysis. The clusterProfiler R package [23] was used to annotate the genes pattern. The consensus clustering algorithm [18] was performed to define the gene clusters. The Chi-square contingency test was used to determine the correlation between the metabolic clusters and gene clusters. Next, we applied an L1-penalized (Lasso) regression to further identify the DEGs with independent prognostic value [24]. Based on

the highest lambda value that was selected through 1000 cross-validations in the Lasso method ('11 min' lambda), we obtained a set of prognostic genes and their Lasso regression coefficients.

$$\text{Risk score} = -0.0188 * \text{SFTPB} (\text{gene expression level}) + (-0.0034 * \text{CYP4B1}) + 0.0258 * \text{CDKN3} + (-0.0128 * \text{CLEC3B}) + 0.0305 * \text{ABCC2} + 0.1003 * \text{DLGAP5} + 0.0295 * \text{HPGD} + 0.0258 * \text{SERPINB5} + (-0.0923 * \text{MS4A1}) + 0.0400 * \text{MUC1} + 0.0654 * \text{KYNU} + 0.0003 * \text{CST6} + 0.0211 * \text{CPS1} + 0.0092 * \text{IGF2BP3} + \text{NTS} * 0.0071.$$

## Pathway enrichment analysis

All gene sets were downloaded from the MSigDB database [25]. Gene set variation analysis (GSVA) was performed on the metabolic gene signatures, gene clusters and metabolic score using the clusterProfiler R package [26]. Pathways enriched in metabolic-related gene clusters were identified in Gene Ontology (GO) enrichment analysis with the false discovery rate (FDR)  $< 0.05$  and a strict cutoff value of  $P < 0.01$ .

## Genomic alteration analysis

RNA-seq data in regard to somatic copy number alternations (CNAs) and somatic mutations were downloaded from the TCGA database. GSITIC analysis was performed to determine the specific genomic event enrichment. CNAs and the threshold copy number (CN) at alteration peaks associated with metabolic score were from GISTIC 2.0 analysis (<https://gatkforums.broadinstitute.org>). The first 25% and the last 25% of samples were adopted to perform GISTIC analysis.

## Prediction of immunotherapy response

The Tumor Immune Dysfunction and Exclusion (TIDE) algorithm was performed to infer individual responses to immunotherapy, e.g., anti-PD-1 therapy [27, 28]. The submap analysis was applied to show the difference in response to anti-PD-1 and CTLA-4 therapy. For the urothelial cancer dataset (IMvigor,  $n = 298$ ), the data package was downloaded from <http://research-pub.gene.com/IMvigor210CoreBiologies>. The R package arrayQualityMetrics was used for quality control, and the trimmed mean of  $M$ -values was used for normalization of count data [21]. T cell-inflamed gene expression profile (GEP) was defined through the expression of the 18 genes [29].

## Statistical analysis

The Shapiro–Wilk normality test was used to test the normality of the variables [26]. For normally distributed

variables, unpaired Student's *t*-test was used to compare the differences between the two groups. The Wilcoxon test was used to compare non-normally distributed variables. For multiple groups, one-way analysis of variance (ANOVA) was used as a parametric method to compare mean values, while Kruskal–Wallis tests were used as a nonparametric method.

Pearson correlation and distance correlation analyses were used to calculate the correlation coefficients. Contingency tables were analyzed using the Chi-square contingency test. The overall survival and Metscore were calculated using the R package survival and cutoff values determined. Based on the dichotomized Metscore, patients were grouped into high or low Metscore in each dataset, while reducing the computational batch effect using the R package sva. Data were mainly visualized using the R package ggplot2. In the differential expressed gene analysis, we used the Benjamini–Hochberg method that converts the *P* values to FDRs to identify significant genes [30]. The receiver operating characteristic package (pROC) [31] was utilized to generate ROC curves and calculate the area under the curve (AUC). OncoPrint was used to delineate the mutation landscape of TCGA via the maftools R package [32]. Lasso regression analysis was used to identify prognostic genes. The Kaplan–Meier method was applied to generate and visualize survival curves for the subgroups. The statistical significance of differences in each dataset was determined by the log-rank test. The univariate and multivariate Cox proportional hazards regression models were utilized to calculate the hazard ratios in the univariate and multivariate analyses and determine independent prognostic factors employing the R package survival. All survivorship curves were generated via R package survminer. All heatmaps were generated based on pheatmap. All statistical analyses were performed in R (<https://www.r-project.org/version.3.6.1>). All the tests were two-sided, and  $P < 0.05$  were considered statistically significant.

## Results

### Kmdist identifies two subclasses in LUAD

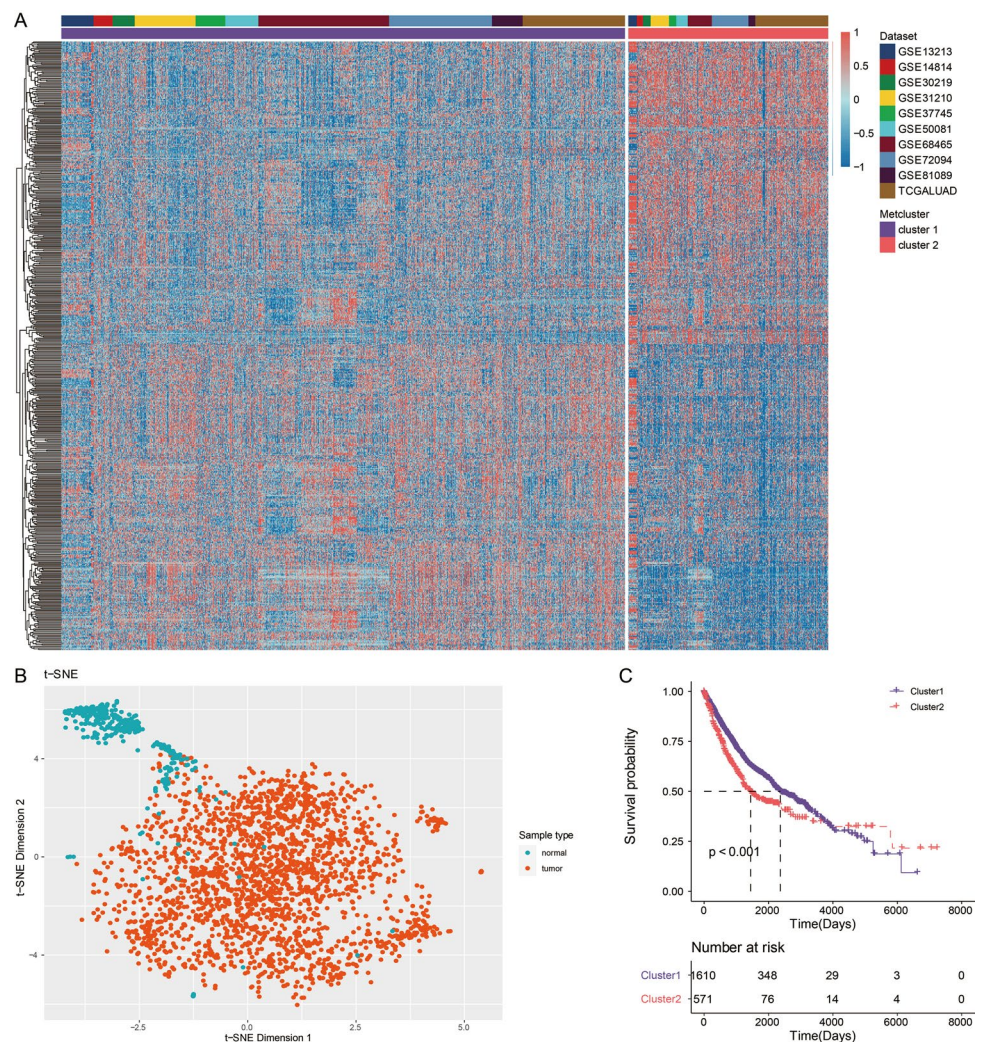
Figure S1A shows a flowchart developed to systematically describe our study. In total, 559 candidate metabolic genes were identified for clustering. The batch effect of the included cohorts before and after sva reduction is shown in Figs. S1B and S1C, respectively. The clustering stability was assessed using the ConsensusClusterPlus package in the meta-cohorts based on the 559 genes for the optimal cluster number (Supplementary Fig. S1D). This supported two robust subtypes of LUAD in meta-cohorts.

Kmdist of the 2181 tumors with corresponding metabolic gene expression profiles in meta-cohorts was performed (Fig. 1a and Supplementary Table S1). We also performed t-SNE to validate the subclasses' assignments and found that the 559 metabolic genes separated tumor and normal tissues (Fig. 1b and Supplementary Table S2). Two identified metabolic phenotypes showed significant differences in the OS in meta-cohorts (log-rank test,  $P < 0.001$ ; Fig. 1c). Clustering stability was also assessed using the ConsensusClusterPlus package in the TCGA for the optimal cluster number (Supplementary Fig. S1E), which supported two robust subtypes of LUAD in TCGA. The two metabolic clusters were termed as Metclusters. Kmdist of the 500 tumors with corresponding metabolic gene expression profiles in the TCGA was performed (Fig. S2A). Two identified metabolic phenotypes also showed significant differences in the OS in TCGA (log-rank test,  $P < 0.001$ ; Fig. S2B).

### Transcriptome feature of the LUAD subclasses

We further explored the association between the identified metabolic subclasses and the metabolic-related pathways. Kmdist of the 2181 tumors in meta-cohorts was performed based on the 40 identified metabolic-related pathways (Fig. 2a and Supplementary Table S3). The t-SNE analysis also showed that the 40 identified metabolic-related pathways separated tumor and normal tissues (Fig. 2b). Kmdist of the 500 tumors in TCGA was also performed based on the 40 identified metabolic-related pathways (Figs. S2C and Supplementary Table S3). In meta-cohorts and TCGA, Kmdist of the 2181 tumors was further performed based on the 28 immune infiltrating cells (Figs. 2c and S3A, respectively). Figures 2d and S3B reveal that the two metabolic clusters showed significant differences in immune cell infiltration patterns in meta-cohorts and TCGA, respectively. Furthermore, 20 immune-related signaling pathways and tumorigenic-related pathways in GO enrichment analysis (Supplementary Table S4) were identified in meta-cohorts and TCGA (Fig. 3a and S3C, respectively). We also investigated the correlation between the two metabolic clusters and known signatures in both meta-cohorts and TCGA (Figs. 3b and S4A, respectively). Intrinsic immune escape is attributed to the expression of the immune checkpoint molecules, which are classified into several groups including antigen-presenting cells, costimulators, co-inhibitors, receptors, ligands, cell adhesions, etc. [33, 34]. Our results revealed that LUAD in metabolic cluster 1 expressed more immune checkpoint molecules to facilitate escape from immune killing in meta-cohorts and TCGA (Fig. 3c and S4B, respectively).

**Fig. 1** Metabolic genes involved in LUAD meta-cohorts. **a** Unsupervised clustering of metabolic genes for 2181 patients in meta-cohorts. **b** t-distributed stochastic neighbor embedding (t-SNE) analysis based on metabolic genes clearly separated tumor and normal tissue. **c** Kaplan–Meier curves showing the association between Met-clusters and OS of 2181 patients in meta-cohorts (log-rank test,  $P < 0.001$ )



## Generation of metabolic gene signatures and functional annotation

To further investigate the potential biological characteristics of each metabolic cluster, 220 DEGs were acquired (Supplementary Table S5) and used to classify the patients into genomic subtypes. To select the optimal cluster number, clustering stability was assessed using the ConsensusClusterPlus package was used (Supplementary Fig. S4C), which supported two gene clusters of LUAD in TCGA, termed gene cluster 1 and gene cluster 2 (Fig. S5A). The clustering results of the two genomic subtypes were significantly consistent with the clustering results of the metabolic phenotype groups (S6A,  $\chi^2$  contingency tests,  $P < 1.2 \times 10^{-67}$ ). NMF method was used to compare with Metclusters and gene clusters, which showed good consistency (S5B, S5C, P.fisher tests,  $P < 3.7 \times 10^{-49}$ ,  $P < 1.52 \times 10^{-108}$ , respectively). The survival analysis of the two patient clusters indicated that gene cluster 1 correlated with better survival (Fig. S5D). Kmdist of the 500 tumors in TCGA was further performed

based on the 40 identified metabolic-related pathways (Figs. S5E, Supplementary Table S6). Figure S6B reveals that the two gene clusters had significant differences in known signatures in TCGA. The two gene clusters also showed significant differences in immune cell infiltration patterns in TCGA (Fig. S6C). LUAD in gene cluster 1 expressed more immune checkpoint molecules to help escape from immune killing in TCGA (Fig. S6D). The GO enrichment analysis (Supplementary Table S7) showed that gene cluster 1 was involved in immune-related pathways (Fig. S5F), while gene cluster 2 was involved in DNA regulation-related pathways (Fig. S5G).

## Generation of Metscore and its transcriptome traits as well as clinical characteristics

Lasso regression was adopted to analyze the data (Fig. 4a, b). After multiplying gene expression with Lasso coefficient, 15 prognostic genes were achieved: SFTPB, CYP4B1, CDKN3, CLEC3B, ABCC2, DLGAP5, HPGD, SERPINB5,



**Fig. 2** Characteristics of Metclusters in meta-cohorts. **a** Unsupervised clustering of metabolic related pathways for 2181 patients in meta-cohorts. \* $P < 0.05$ ; \*\* $P < 0.01$ ; \*\*\* $P < 0.001$ ; \*\*\*\* $P < 0.0001$ . **b** t-distributed stochastic neighbor embedding (t-SNE) analysis based on metabolic related pathways clearly separated tumor and normal tissue. **c** Unsupervised clustering of immune infiltrating cells for 2181 patients in meta-cohorts. **d** The fraction of immune cells in two meta-

bolic clusters. The scattered dots represent immune cell expression values in each group. The thick line represents the median value. The upper and lower parts of the boxes are the 25th and 75th percentiles (interquartile range), respectively. The whiskers encompass 1.5 times the interquartile range. Difference between two metabolic clusters was compared using the Kruskal–Wallis test. \* $P < 0.05$ ; \*\* $P < 0.01$ ; \*\*\* $P < 0.001$ ; \*\*\*\* $P < 0.0001$

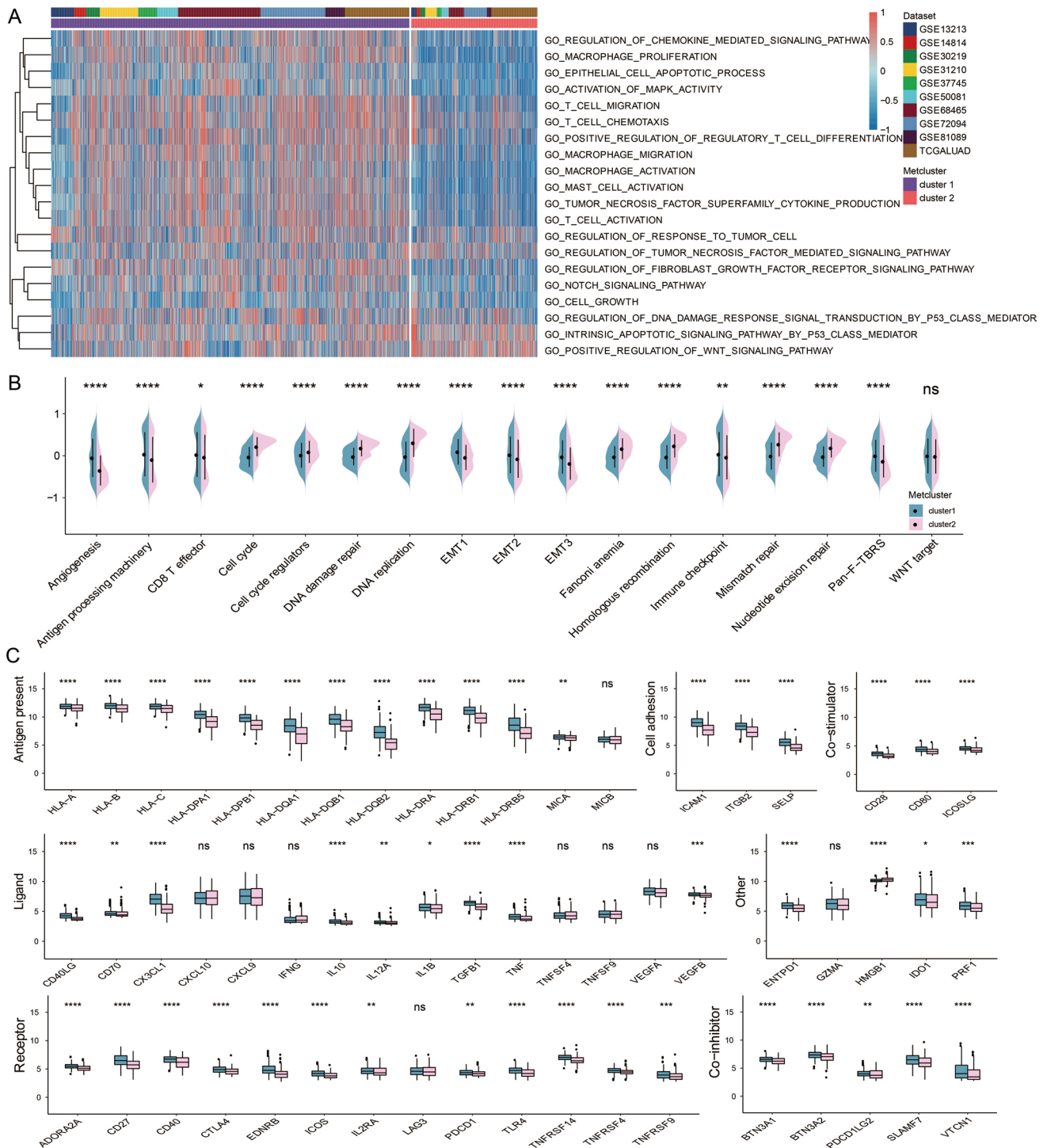


**Fig. 3** Functional annotation of immune related Metclusters in meta-cohorts. **a** GSEA of metabolic clusters based on meta-cohorts in GO. **b** Different known signatures were used to distinguish Metclusters

in meta-cohorts. **c** The expression pattern of seven types of immune checkpoints in Metclusters in meta-cohorts. The scattered dots represent immune checkpoints expression values in each group

MS4A1, MUC1, KYNU, CST6, CPS1, IGF2BP3 and NTS (Fig. 4c and Supplementary Table S8). To select the optimal cluster number, clustering stability was assessed using the ConsensusClusterPlus package based on the 15 genes

(Supplementary Fig. 4d), which supported two lasso gene clusters of LUAD in TCGA, termed Lasso gene cluster 1 and Lasso gene cluster 2. The clustering results of the two lasso gene subtypes were significantly consistent with the

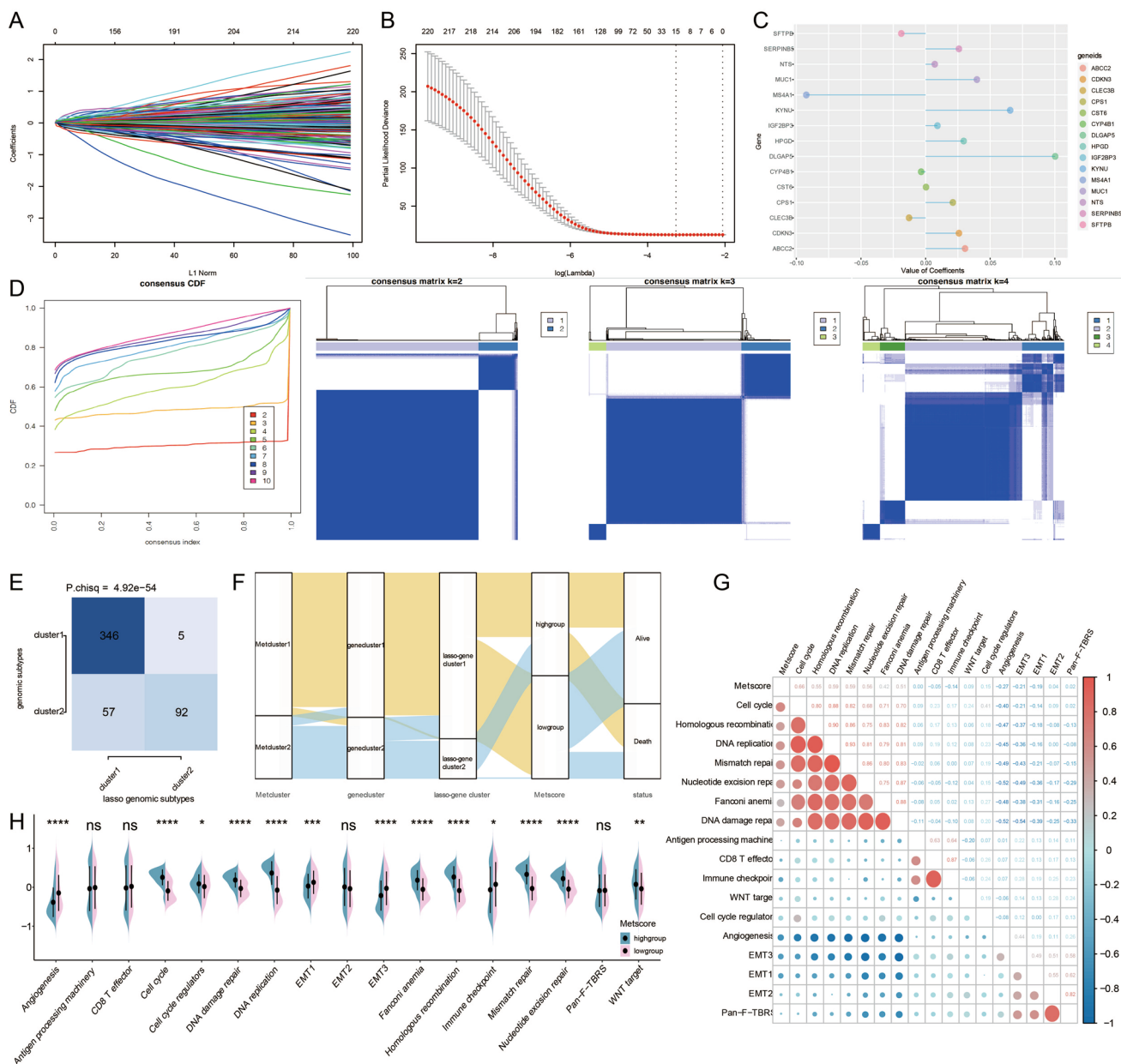


**Fig. 4** Generation of Lasso regression genes. **a** Coefficient value of DEGs. **b** Partial likelihood deviance of DEGs. **c** Coefficient value of 15 prognostic genes. **d** The consensus clustering algorithm defining Lasso-gene clusters. Consensus clustering cumulative distribution function (CDF) for  $k=2-10$  in TCGA. Consensus matrixes of TCGA for each  $k$  ( $k=2-4$ ), displaying the clustering stability using 1000 iterations of hierarchical clustering. **e** Contingency table estimat-

ing the consistency between gene clusters and lasso-gene clusters. **f** Sankey plot illustrating the interconnection among metabolic clusters, metabolic gene clusters, metabolic lasso-gene clusters, Metscore, and patient survival. **g** The correlation between Metscore and known signatures. **h**. Metscore groups were distinguished by different known signatures

clustering results of the genomic subtypes (Fig. 4E,  $\chi^2$  contingency tests,  $P < 4.92 \times 10^{-54}$ ). The t-SNE analysis also showed that the 15 prognostic genes clearly separated tumor and normal tissues (Fig. 5a). The ROC curve further confirmed that the 15 prognostic genes were sensitive markers for separating tumor and normal tissues (Fig. 5b). The metabolic score, termed as Metscore, was calculated

for patients with the 15 prognostic genes and a cutoff value between the high- and low-metabolic-score groups was set at the median value (Supplementary Table S9). The survival analysis indicated that patients with high Metscore correlated with better survival (Fig. 5c). Metabolic cluster 2 had a higher Metscore in both meta-cohorts and TCGA (Fig. 5d and f, respectively). The ROC curve further confirmed that



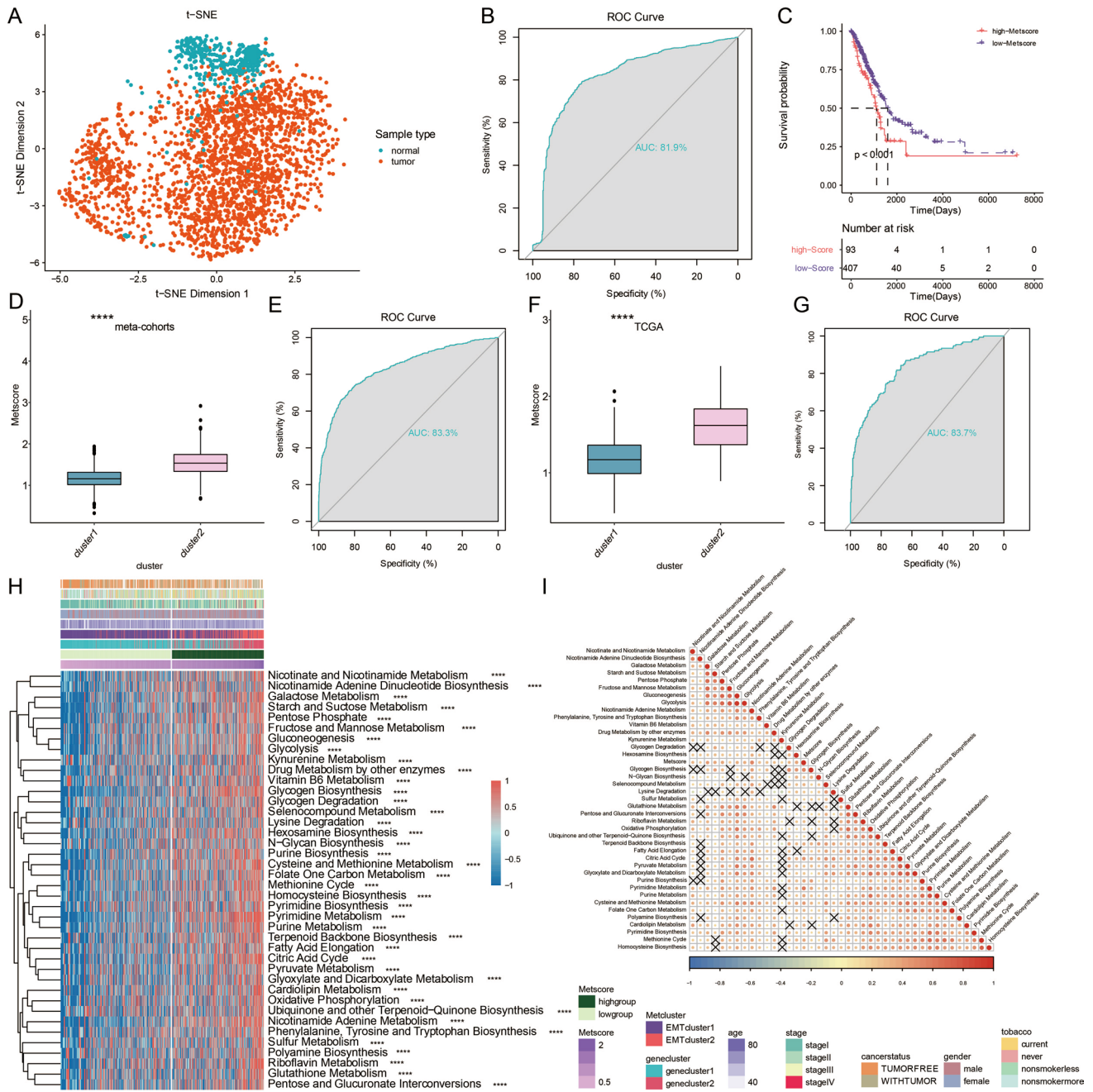


**Fig. 5** Construction of a Metscore. **a** t-distributed stochastic neighbor embedding (t-SNE) analysis based on Lasso genes clearly separated tumor and normal tissue. **b** ROC curve measuring the sensitivity of lasso genes in separating tumor and normal tissue. The area under the ROC curve was 0.819. **c** Kaplan–Meier curves showing the association between Metscore and OS of 500 patients in TCGA (log-rank test,  $P < 0.001$ ). **d** Expression pattern of Metclusters in Metscore in meta-cohorts. **e** ROC curve measuring the consistency

between Metscore and Metclusters in meta-cohorts. **f** Expression pattern of Metclusters in Metscore in TCGA. **g** ROC curve measuring the consistency between Metscore and Metclusters in TCGA. **h** Unsupervised clustering of metabolic related pathways for 500 patients in TCGA database.  $*P < 0.05$ ;  $**P < 0.01$ ;  $***P < 0.001$ ;  $****P < 0.0001$ . **i** Correlation between Metscore and 40 known metabolic signatures

the Metscore was a sensitive marker for metabolic clusters (Fig. 5e and g, respectively). The interconnection among the metabolic clusters, metabolic gene clusters, metabolic lasso gene clusters, Metscore and patient survival is illustrated

in the Sankey plot (Fig. 4f). Kmdist of the 500 tumors in TCGA was further performed based on the 40 identified metabolic-related pathways (Fig. 5h, and Supplementary Table S10). The correlation of the Metscore with 40 known

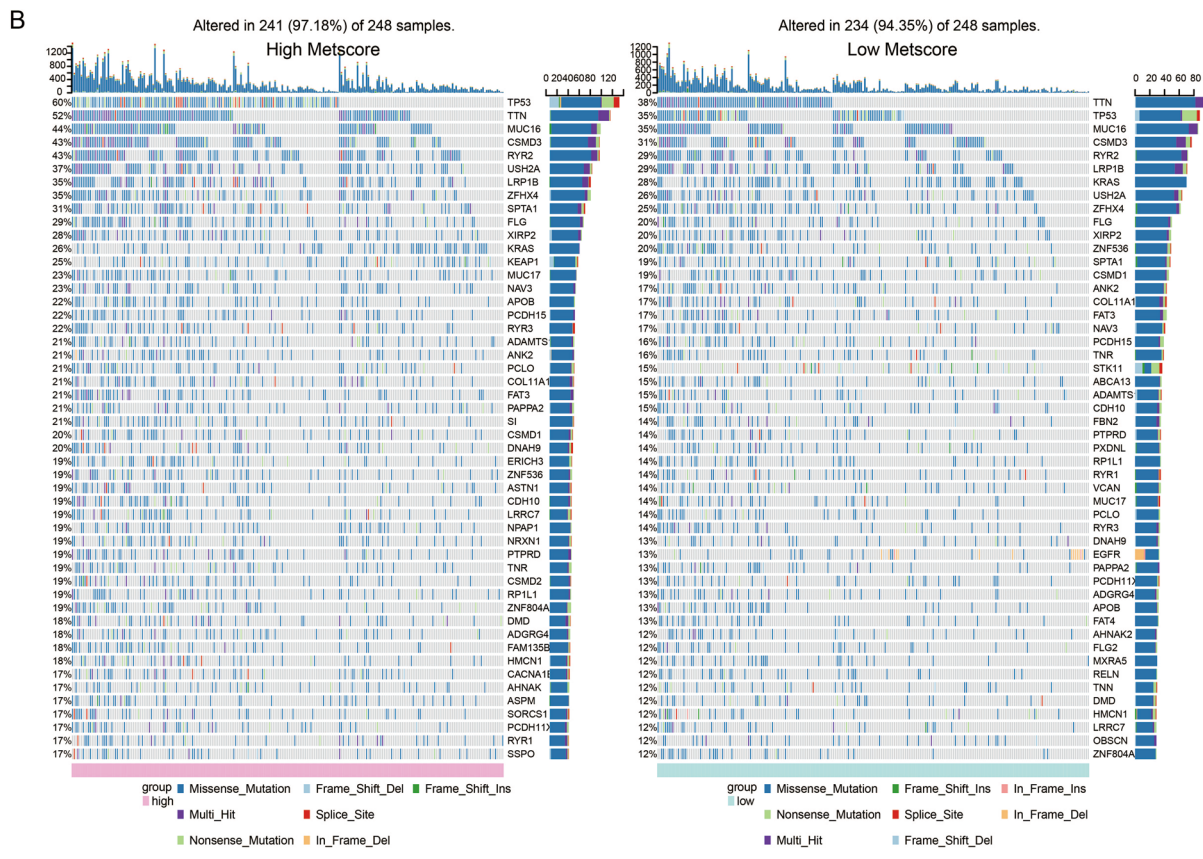
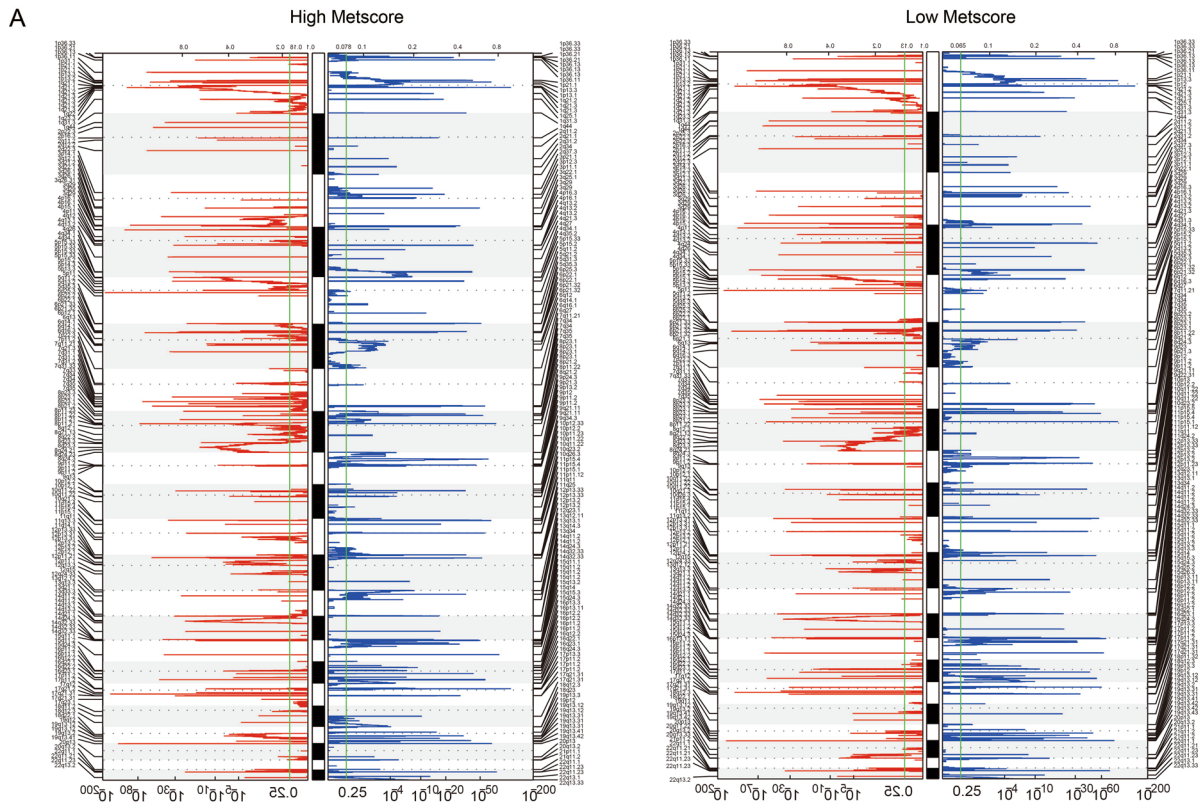


**Fig. 6** Distinct genomic profiles associated with Metscore. **a** GIS-TIC 2.0 amplifications and deletions in LUAD with high Metscore and low Metscore. Chromosomal locations of peaks corresponding to the significantly recurring focal amplification (red) and deletions (blue). **b** Differential somatic mutations in LUAD with low and high Metscores

metabolic signatures is shown in Fig. 5l. The two Metscore groups showed significant differences in known signatures in TCGA (Fig. 4h). The correlation between the Metscore and known signatures is shown in Fig. 4g. The two Metscore groups also showed significant differences in the immune cell infiltration patterns in TCGA (Fig. S7A). The correlation between the Metscore and immune cell infiltration patterns is shown in Fig. S7B. Furthermore, 20 immune-related signaling pathways and tumorigenic-related pathways in the GO enrichment analysis (Supplementary Table S11) were identified in TCGA with regard to Metscore (Fig. S7C).

### Metscore is associated with unique patterns of genomic alterations

To determine the association between Metscore and LUAD genomic profiles, CNA and somatic mutation analysis were performed in the TCGA dataset. In the high-Metscore samples, frequently amplified genomic regions containing oncogenic driver genes and immune regulatory genes, including NRAS (1p13.27), DUP3Q29 (3q29), LYZ (5p11), HLA-DQA1 (6p21.32), CHEK2P2 (15q11.1), STAT3 (17q21.2) and KLK3 (19q13.33), were associated with COL11A1 (1p21.1), MCL1 (1q21.2), UGT2B7 (4q13.2), ANGPT2 (8p23.1), PTEN (10q23.31), TNFRSF13B (17p11.2), TNNT3 (19q13.42) and GSTT1 (22q11.23) deletion peaks (Fig. 6a). Furthermore, analysis of somatic mutation profiles indicated a high frequency of mutations in TP53 (60%), TTN (52%), MUC16 (44%), CSMD3 (43%), RYR2 (43%), USH2A (37%), LRP1B (35%), ZFHX4 (35%) and SPTA1 (31%) in the high Metscore, while TTN (38%), TTN (35%), MUC16 (29%) and CSMD (31%) showed higher-frequency mutations in the low Metscore cluster (Fig. 6b).

### Metscore predicts therapeutic benefits

The prognostic value of the Metscore in the TCGA-LUAD cohort was assessed. Metscore was a risk factor in multiple cancers (Fig. 7a). The expression difference of Metscore in several clinical factors, including tumor stage, smoking, gender, cancer status and patient age, is shown in Supplementary Fig. S10A. Metscore and tumor stage served as hazardous prognostic markers based on the univariate analysis in TCGA (Fig. 7b), while Metscore, tumor stage and smoking served as hazardous markers based on multivariate analysis in TCGA (Fig. 7c). Survival analysis of

Metscore in the 10 included cohorts was determined. A high Metscore exhibited worse survival in all datasets (Fig. S8). Further, Metscore predicted worse survival in all included LUAD samples (Fig. 7d). Metscore was also verified in an external LUAD cohort, GSE87340, which Metscore significantly stratified LUAD patients and served as a hazardous marker (Fig. 7e). In the pan-cancer analysis, high Metscore was found to be correlated with poor survival in BLCA, BRCA, READ, SKCM, HNSC, KIRC, LGG, LIHC and THCA (Fig. S9). The potential response to immunotherapy in TCGA based on the TIDE algorithm was evaluated. The results showed that patients with low Metscore had a better response to immunotherapy compared to those with high Metscore (Fig. 7f). Subsequently, the response to anti-PD-1 and anti-CTLA-4 therapy was analyzed. The results showed that the low-Metscore group had a better response to anti-PD-1 immunotherapy (Fig. 7g). In the urothelial cancer dataset, patients with high Metscore had significantly shorter OS than those with lower Metscore in the IMvigor210 cohort (Fig. 7h). Given the critical role of cancer-related fibroblasts (CAFs) in immune escape, the correlation between CAF and Metscore was explored, and high Metscore had higher level of CAF (Fig. 7i). Previous studies have demonstrated that T cell-inflamed GEP can induce IFN- $\gamma$ -related response genes, cytotoxic activity (CYT), chemokine expression and adaptive immune resistance, which are also associated with the response to anti-PD-1 therapy [29]. We analyzed the potential correlation between Metscore and GEP. The results demonstrated that Metscore was significantly associated with GEP (Fig. 7j). Metcluster 1, gene cluster 1 and high Metscore all indicated high expression of GEP (Fig. 7k). Aneuploidy, also known as somatic copy number alterations (SCNAs), has been proposed to drive tumorigenesis in multiple cancers [35]. In this study, a high Metscore was associated with lower arm SCNA level, chromosome SCNA level and focal SCNA level (Fig. S10B).

### Discussion

In this work, we classified patients into two groups: Metcluster 1 and Metcluster 2, based on metabolism-related gene expression to study the relationship between tumor metabolic pattern and tumor microenvironment. Differential activated metabolism-related pathways were identified between the two clusters. For example, lipid metabolism-related pathways were enriched in Metcluster 1 (the low-risk group), while glucose and amino acid metabolism were activated in Metcluster 2 (the high-risk group). Critically, immunocytes infiltration of the cytotoxic immunocytes (including regulatory T cells, NK cells, CD8 + T cells and macrophage), and antigen, immune ligand and immune receptor expression were higher in Metcluster 1 compared to Metcluster 2.

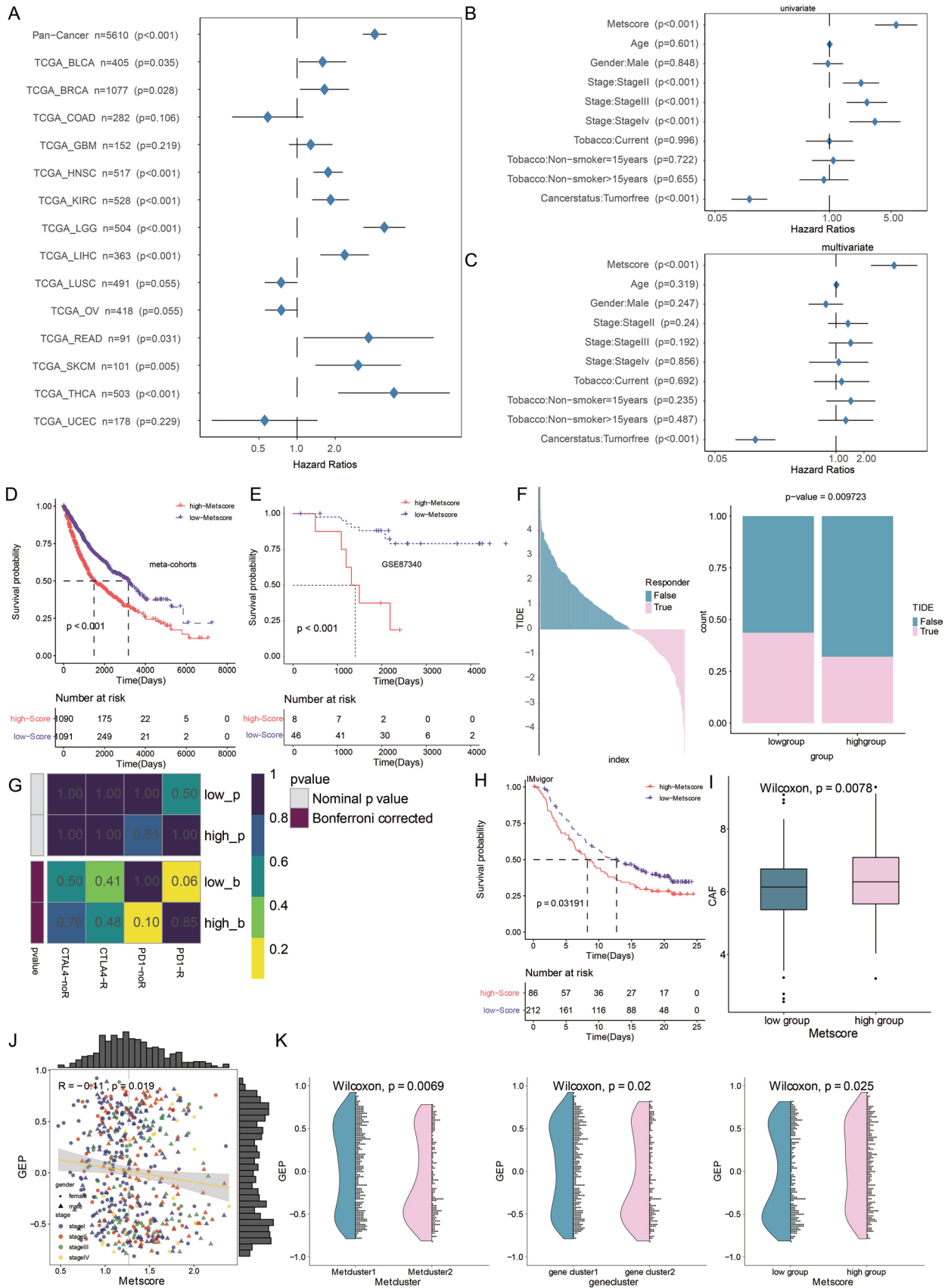


**Fig. 7** Metscore is a prognostic biomarker that predicts immunotherapeutic benefit. **a** Subgroup analyses estimating the prognostic value of Metscore in different types of cancer from TCGA. The length of horizontal line represents the 95% confidence interval for each group. The vertical dotted line represents the HR of all patients. HR < 1.0 indicates that high Metscore is a favorable prognostic biomarker for the indicated number of patients. **b** Univariate cox regression analysis and **c** multivariate cox regression analysis performed to estimate the clinical prognostic factors (including Metscore) of TCGA. **d** Kaplan–Meier curves showing the association between Metscore and OS of meta-cohorts (log-rank test,  $P < 0.001$ ). **e** Kaplan–Meier curves showing the association between Metscore and OS of GSE87340 (log-rank test,  $P < 0.001$ ). **f** The TIDE value and response to immunotherapy of patients with Metscore. **g** Submap analysis based on the TIDE algorithm showed significant differences in response to CTAL-4 and anti-PD-1 therapy across different Metscores in TCGA database. **h** Kaplan–Meier curves showing the association between Metscore and OS of IMvigor dataset (log-rank test,  $P = 0.03191$ ). **i** The expression difference of CAF in Metscore groups (Wilcoxon,  $P = 0.0078$ ). **j** The correlation between GEP and Metscore. Pearson Correlation Coefficient  $R = -0.11$ . **k** The difference in expression of GEP across Met-clusters, gene clusters, and Metscore groups. The differences between groups were compared using the Wilcoxon test (Wilcoxon,  $P < 0.001$ )

Thus, to further explore the relationship between the cluster model and tumor immune landscape, we qualify the cluster model by constructing a scoring system, Metscore.

Previous studies confirmed that the components of tumor microenvironment contribute to tumor resistance to immunotherapy [8, 36, 37]. For instance, the infiltration ratio of immunocytes such as T cells, regulatory T cells and NK cells has been proved to modulate tumor sensitivity to immunotherapy [38, 39]. Cancer-associated fibroblasts express PD-1 and PD-L1 to suppress immunocytes' function [40]. The density of the extracellular matrix affects tumor response to immunotherapy by influencing T cells infiltration [41]. Importantly, we discovered that high-Metscore samples showed more disordered TME than low-Metscore samples.

TME has been proved to affect tumor response to immunotherapy by defining tumor as 'hot' or 'cold' based on the components of TME [42, 43]. 'Hot' tumor (more sensitive to immunotherapy) shows signs of inflammation and is infiltrated with immunocytes, while a 'cold' tumor is barely infiltrated with immunocytes and lacks immune response [44]. In this work, samples from low-Metscore group are more sensitive to anti-PD-1 immunotherapy compared to the high-Metscore group, and tumor with a low Metscore is more likely to be classified as a 'hot' tumor. Therefore, reprogramming a 'cold' tumor by modulating immune system activation can improve tumor response to immunotherapy.

Recently, metabolic patterns of tumor cells have been gradually recognized as critical regulators of TME, which might affect tumor response to immunotherapy [9, 45]. Increased glycolysis-related molecules in tumor cells impair T cells function and proliferation [46, 47]. Tumor cells induced T cells function suppression by increasing tryptophan absorption [48]. In melanoma, activated lipid

metabolism increased tumor sensitivity to immunotherapy by upregulating antigen expression [49]. In this work, different metabolic patterns of tumor cells between high- and low-Metscore samples are also identified further supporting the association between tumor metabolic pattern and tumor immune landscape.

Compared with the previously established metabolic related prognostic models [50, 51], more abundant LUAD samples were used for the construction of Metscores to ensure its reliability. However, the validation cohort should be constructed by additional samples to confirm this reliability. In this work, high-Metscore group showed worse survival outcomes, but its prognostic value still needs to compare with biomarkers like EGFR or KRAS. The Metscore model is associated with the activation of glucose and amino acid metabolism-related pathways and higher T cell-inflamed gene expression implying this scoring system may be beneficial in guiding LUAD immunotherapy. Nevertheless, the association between different metabolic pattern and immunocytes' function also required deeper exploration. The model's efficiency in evaluating lung cancer immunotherapy should also be confirmed in future clinical trial.

**Supplementary Information** The online version contains supplementary material available at <https://doi.org/10.1007/s00262-021-02896-6>.

**Authors' contributions** XW, DS, YM, MX, HZ, ZW and ZN designed and drafted the manuscript; LL, PL, JJ, JY and DL wrote figure legends and revised the article; HC, ZX and QC conducted the data analysis; All authors read and approved the final manuscript.

**Funding** This work was supported by Anhui Provincial Natural Science Foundation (No. 1808085QH270; 2008085QH428) and 'the Fundamental Research Funds for the Central Universities' (No. WK9110000121). This work was supported by the National Natural Science Foundation of China (Nos. 82073893; 81703622), China, Post-doctoral Science Foundation (No. 2018M633002), Hunan Provincial Natural Science Foundation of China (No. 2018JJ3838), Hunan Provincial Health Committee Foundation of China (No. C2019186) and Xiangya Hospital Central South University postdoctoral foundation.

**Data availability** All data used in this work can be acquired from the Gene Expression Omni-bus (GEO; <https://www.ncbi.nlm.nih.gov/geo/>), the Cancer Genome Atlas (TCGA) datasets (<https://xenabrowser.net/>).

## Compliance with ethical standards

**Conflict of interest** All authors declare that they have no conflict of interest.

## References


1. Bade BC, Dela Cruz CS, Cancer L (2020) Epidemiology, etiology, and prevention. *Clin Chest Med* 41(2020):1–24

2. Myers DJ, Wallen JM (2020) Lung Adenocarcinoma. StatPearls Publishing, Treasure Island, FL. Available from: <https://www.ncbi.nlm.nih.gov/books/NBK519578/>
3. Herbst RS, Baas P, Kim DW, Felip E, Perez-Gracia JL, Han JY, Molina J, Kim JH, Arvis CD, Ahn MJ, Majem M, Fidler MJ, de Castro G, Jr., Garrido M, Lubiniecki GM, Shentu Y, Im E, Dolled-Filhart M, Garon EG (2016) Pembrolizumab versus docetaxel for previously treated, PD-L1-positive, advanced non-small-cell lung cancer (KEYNOTE-010): a randomised controlled trial. *Lancet* 387:1540–1550
4. Borghaei H, Paz-Ares L, Horn L, Spigel DR, Steins M, Ready NE, Chow LQ, Vokes EE, Felip E, Holgado E, Barlesi F, Kohlhaufl M, Arrieta O, Burgio MA, Fayette J, Lena H, Poddubskaya E, Gerber DE, Gettinger SN, Rudin CM, Rizvi N, Crino L, Blumenschein GR Jr, Antonia SJ, Dorange C, Harbison CT, Graf Finckenstein F, Brahmer JR (2015) Nivolumab versus docetaxel in advanced nonsquamous non-small-cell lung cancer. *N Engl J Med* 373:1627–1639
5. Li J, He Y, Tan Z, Lu J, Li L, Song X, Shi F, Xie L, You S, Luo X, Li N, Li Y, Liu X, Tang M, Weng X, Yi W, Fan J, Zhou J, Qiang G, Qiu S, Wu W, Bode AM, Cao Y (2018) Wild-type IDH2 promotes the Warburg effect and tumor growth through HIF1alpha in lung cancer. *Theranostics* 8:4050–4061
6. Chang CH, Qiu J, O'Sullivan D, Buck MD, Noguchi T, Curtis JD, Chen Q, Gindin M, Gubin MM, van der Windt GJ, Tonc E, Schreiber RD, Pearce EJ, Pearce EL (2015) Metabolic competition in the tumor microenvironment is a driver of cancer progression. *Cell* 162:1229–1241
7. Ho PC, Bihuniak JD, Macintyre AN, Staron M, Liu X, Amezcua R, Tsui YC, Cui G, Micevic G, Perales JC, Kleinstein SH, Abel ED, Insogna KL, Feske S, Locasale JW, Bosenberg MW, Rathmell JC, Kaech SM (2015) Phosphoenolpyruvate is a metabolic checkpoint of anti-tumor T cell responses. *Cell* 162:1217–1228
8. Ramapriyan R, Caetano MS, Barsoumian HB, Mafra ACP, Zambalde EP, Menon H, Tsouko E, Welsh JW, Cortez MA (2019) Altered cancer metabolism in mechanisms of immunotherapy resistance. *Pharmacol Ther* 195:162–171
9. Li X, Wenes M, Romero P, Huang SC, Fendt SM, Ho PC (2019) Navigating metabolic pathways to enhance antitumor immunity and immunotherapy. *Nat Rev Clin Oncol* 16:425–441
10. Lim SM, Hong MH, Kim HR (2020) Immunotherapy for non-small cell lung cancer: current landscape and future perspectives. *Immune Netw* 20:10
11. Raju S, Joseph R, Sehgal S (2018) Review of checkpoint immunotherapy for the management of non-small cell lung cancer. *Immunotargets Ther* 7:63–75
12. Bradbury PA, Shepherd FA (2008) Immunotherapy for lung cancer. *J Thorac Oncol* 3:S164–S170
13. Hsu ML, Naidoo J (2020) Principles of immunotherapy in non-small cell lung cancer. *Thorac Surg Clin* 30:187–198
14. Barrieto L, Caminero F, Cash L, Makris C, Lamichhane P, Deshmukh RR (2020) Resistance to checkpoint inhibition in cancer immunotherapy. *Transl Oncol* 13:100738
15. Faruki H, Mayhew GM, Serody JS, Hayes DN, Perou CM, Lai-Goldman M (2017) Lung adenocarcinoma and squamous cell carcinoma gene expression subtypes demonstrate significant differences in tumor immune landscape. *J Thorac Oncol* 12:943–953
16. Possemato R, Marks KM, Shaul YD, Pacold ME, Kim D, Birsoy K, Sethumadhavan S, Woo HK, Jang HG, Jha AK, Chen WW, Barrett FG, Stransky N, Tsun ZY, Cowley GS, Barretina J, Kalaany NY, Hsu PP, Ottina K, Chan AM, Yuan B, Garraway LA, Root DE, Mino-Kenudson M, Brachtel EF, Driggers EM, Sabatini DM (2011) Functional genomics reveal that the serine synthesis pathway is essential in breast cancer. *Nature* 476:346–350
17. Ball GH, Hall DJ (1967) A clustering technique for summarizing multivariate data. *Behav Sci* 12:153–155
18. Monti S, Tamayo P, Mesirov J, Golub T (2003) Consensus clustering: a resampling-based method for class discovery and visualization of gene expression microarray data. *Mach Learn* 52(1):91–118
19. Hanzelmann S, Castelo R, Guinney J (2013) GSEA: gene set variation analysis for microarray and RNA-seq data. *BMC Bioinformatics* 14:7
20. Charoentong P, Finotello F, Angelova M, Mayer C, Efremova M, Rieder D, Hackl H, Trajanoski Z (2017) Pan-Cancer immunogenomic analyses reveal genotype-immunophenotype relationships and predictors of response to checkpoint blockade. *Cell Rep* 18:248–262
21. Ritchie ME, Phipson B, Wu D, Hu Y, Law CW, Shi W, Smyth GK (2015) Limma powers differential expression analyses for RNA-sequencing and microarray studies. *Nucleic Acids Res* 43:47
22. Hartigan JA, Wong MA (1979) Algorithm as 136 A K-means clustering algorithm. *J R Stat Soc Ser C Appl Stat* 28(1):100–108
23. Yu G, Wang LG, Han Y, He QY (2012) ClusterProfiler: an R package for comparing biological themes among gene clusters. *Omics J Integr Bio* 16:284–287
24. Goeman JJ (2010) L1 penalized estimation in the Cox proportional hazards model. *Biom J* 52:70–84
25. Subramanian A, Tamayo P, Mootha VK, Mukherjee S, Ebert BL, Gillette MA, Paulovich A, Pomeroy SL, Golub TR, Lander ES, Mesirov JP (2005) Gene set enrichment analysis: a knowledge-based approach for interpreting genome-wide expression profiles. *Proc Natl Acad Sci U S A* 102:15545–15550
26. Ghasemi A, Zahediasl S (2012) Normality tests for statistical analysis: a guide for non-statisticians. *Int J Endocrinol Metab* 10:486–489
27. Jiang P, Gu S, Pan D, Fu J, Sahu A, Hu X, Li Z, Traugh N, Bu X, Li B, Liu J, Freeman GJ, Brown MA, Wucherpfennig KW, Liu XS (2018) Signatures of T cell dysfunction and exclusion predict cancer immunotherapy response. *Nat Med* 24:1550–1558
28. Lu X, Jiang L, Zhang L, Zhu Y, Hu W, Wang J, Ruan X, Xu Z, Meng X, Gao J, Su X, Yan F (2019) Immune signature-based subtypes of cervical squamous cell carcinoma tightly associated with human papillomavirus type 16 expression. *Mol Features Clin Outcome, Neoplasia* 21:591–601
29. Ayers M, Lunceford J, Nebozhyn M, Murphy E, Loboda A, Kaufman DR, Albright A, Cheng JD, Kang SP, Shankaran V, Piha-Paul SA, Yearley J, Seiwert TY, Ribas A, McClanahan TK (2017) IFN-gamma-related mRNA profile predicts clinical response to PD-1 blockade. *J Clin Invest* 127:2930–2940
30. Benjamini Y, Hochberg Y (1995) Controlling the false discovery rate: a practical and powerful approach to multiple testing. *J R Stat Soc* 57(1):289–300
31. Robin X, Turck N, Hainard A, Tiberti N, Lisacek F, Sanchez J-C, Müller M (2011) Proc: an open-source package for R and S+ to analyze and compare ROC curves. *BMC Bioinform* 12:77
32. Matthias S (2016) Complex heatmaps reveal patterns and correlations in multidimensional genomic data. *Bioinformatics* 32:2847
33. Schreiber RD, Old LJ, Smyth MJ (2011) Cancer immunoeediting: integrating immunity's roles in cancer suppression and promotion. *Science* 331:1565–1570
34. Wang S, Zhang Q, Yu C, Cao Y, Zuo Y, Yang L (2020) Immune cell infiltration-based signature for prognosis and immunogenomic analysis in breast cancer. *Brief Bioinform*. <https://doi.org/10.1093/bib/bbaa026>
35. Davoli T, Uno H, Wooten EC, Elledge SJ (2017) Tumor aneuploidy correlates with markers of immune evasion and with reduced response to immunotherapy. *Science*. <https://doi.org/10.1126/science.aaf8399>

36. Datta M, Coussens LM, Nishikawa H, Hodi FS, Jain RK (2019) Reprogramming the tumor microenvironment to improve immunotherapy: emerging strategies and combination therapies. *Am Soc Clin Oncol Educ Book* 39:165–174
37. Havel JJ, Chowell D, Chan TA (2019) The evolving landscape of biomarkers for checkpoint inhibitor immunotherapy. *Nat Rev Cancer* 19:133–150
38. Sokratous G, Polyzoidis S, Ashkan K (2017) Immune infiltration of tumor microenvironment following immunotherapy for glioblastoma multiforme. *Hum Vaccin Immunother* 13:2575–2582
39. Altorki NK, Markowitz GJ, Gao D, Port JL, Saxena A, Stiles B, McGraw T, Mittal V (2019) The lung microenvironment: an important regulator of tumour growth and metastasis. *Nat Rev Cancer* 19:9–31
40. Nazareth MR, Broderick L, Simpson-Abelson MR, Kelleher RJ Jr, Yokota SJ, Bankert RB (2007) Characterization of human lung tumor-associated fibroblasts and their ability to modulate the activation of tumor-associated T cells. *J Immunol* 178:5552–5562
41. Salmon H, Franciszkiwicz K, Damotte D, Dieu-Nosjean MC, Validire P, Trautmann A, Mami-Chouaib F, Donnadiou E (2012) Matrix architecture defines the preferential localization and migration of T cells into the stroma of human lung tumors. *J Clin Invest* 122:899–910
42. Liu F, Qin L, Liao Z, Song J, Yuan C, Liu Y, Wang Y, Xu H, Zhang Q, Pei Y, Zhang H, Pan Y, Chen X, Zhang Z, Zhang W, Zhang B (2020) Microenvironment characterization and multi-omics signatures related to prognosis and immunotherapy response of hepatocellular carcinoma. *Exp Hematol Oncol* 9:10
43. Galon J, Bruni D (2019) Approaches to treat immune hot altered and cold tumours with combination immunotherapies. *Nat Rev Drug Discov* 18:197–218
44. Rodallec A, Sicard G, Fanciullino R, Benzekry S, Lacarelle B, Milano G, Ciccolini J (2018) Turning cold tumors into hot tumors: harnessing the potential of tumor immunity using nanoparticles. *Expert Opin Drug Metab Toxicol* 14:1139–1147
45. Zhang J, Shi Z, Xu X, Yu Z, Mi J (2019) The influence of microenvironment on tumor immunotherapy. *FEBS J* 286:4160–4175
46. Cascone T, McKenzie JA, Mbofung RM, Punt S, Wang Z, Xu C, Williams LJ, Wang Z, Bristow CA, Carugo A, Peoples MD, Li L, Karpinets T, Huang L, Malu S, Creasy C, Leahey SE, Chen J, Chen Y, Pelicano H, Bernatchez C, Gopal YNV, Heffernan TP, Hu J, Wang J, Amaria RN, Garraway LA, Huang P, Yang P, Wistuba SE II, Woodman J, Roszik RE, Davis MA, Davies JV, Heymach P, Hwu W. Peng (2018) Increased tumor glycolysis characterizes immune resistance to adoptive T cell therapy. *Cell Metab* 27(5):977–987
47. Afonso J, Santos LL, Longatto-Filho A, Baltazar F (2020) Competitive glucose metabolism as a target to boost bladder cancer immunotherapy. *Nat Rev Urol* 17:77–106
48. Amobi A, Qian F, Lugade AA, Odunsi K (2017) Tryptophan catabolism and cancer immunotherapy targeting IDO mediated immune suppression. *Adv Exp Med Biol* 1036:129–144
49. Harel M, Ortenberg R, Varanasi SK, Mangalharra KC, Mardamshina M, Markovits E, Baruch EN, Tripple V, Arama-Chayoth M, Greenberg E, Shenoy A, Ayasun R, Knafo N, Xu S, Anafi L, Yanovich-Arad G, Barnabas GD, Ashkenazi S, Besser MJ, Schachter J, Bosenberg M, Shadel GS, Barshack I, Kaech SM, Markel G, Geiger T (2019) Proteomics of melanoma response to immunotherapy reveals mitochondrial dependence. *Cell* 179(1):236–250
50. Li S, Xuan Y, Gao B, Sun X, Miao S, Lu T, Wang Y, Jiao W (2018) Identification of an eight-gene prognostic signature for lung adenocarcinoma. *Cancer Manag Res* 10:3383–3392
51. Sun S, Guo W, Wang Z, Wang X, Zhang G, Zhang H, Li R, Gao Y, Qiu B, Tan F, Gao Y, Xue Q, Gao S, He J (2020) Development and validation of an immune-related prognostic signature in lung adenocarcinoma. *Cancer Med* 9:5960–5975

**Publisher's Note** Springer Nature remains neutral with regard to jurisdictional claims in published maps and institutional affiliations.

## Authors and Affiliations

Xian-Ning Wu<sup>1</sup> · Dan Su<sup>2</sup> · Yi-De Mei<sup>3</sup> · Mei-Qing Xu<sup>1</sup> · Hao Zhang<sup>4</sup> · Ze-Yu Wang<sup>4</sup> · Li-Ling Li<sup>6,7</sup> · Li Peng<sup>8</sup> · Jun-Yi Jiang<sup>9</sup> · Jia-Yi Yang<sup>10</sup> · Dong-Jie Li<sup>11,12</sup> · Hui Cao<sup>13</sup> · Zhi-Wei Xia<sup>14</sup> · Wen-Jing Zeng<sup>16</sup> · Quan Cheng<sup>4,15,16</sup>  · Nan Zhang<sup>5</sup>

<sup>1</sup> Department of Thoracic Surgery, The First Affiliated Hospital of USTC, Division of Life Sciences and Medicine, University of Science and Technology of China, Hefei 230001, Anhui, People's Republic of China

<sup>2</sup> School of Nursing, Anhui Medical University, Hefei, People's Republic of China

<sup>3</sup> School of Life Sciences, University of Science and Technology of China (USTC), Hefei 230027, Anhui, People's Republic of China

<sup>4</sup> Department of Neurosurgery, Xiangya Hospital, Central South University, Changsha 410008, People's Republic of China

<sup>5</sup> One-Third Lab, College of Bioinformatics Science and Technology, Harbin Medical University, Harbin 150000, Hei Longjiang, People's Republic of China

<sup>6</sup> Department of Pathology, Xiangya Hospital, Central South University, Changsha, People's Republic of China

<sup>7</sup> Department of Pathology, Xiangya Medical School, Central South University, Changsha, People's Republic of China

<sup>8</sup> Department of Ophthalmology, Central South University Xiangya School of Medicine Affiliated Haikou Hospital, Haikou, People's Republic of China

<sup>9</sup> Aier School of Ophthalmology, Central South University, Changsha, People's Republic of China

<sup>10</sup> Department of Geriatrics, Xiangya Hospital, Central South University, Changsha, People's Republic of China

<sup>11</sup> Department of Clinical Pharmacology, and Geriatric Urology, Xiangya International Medical Center, Xiangya Hospital, Central South University, Changsha, People's Republic of China

- <sup>12</sup> National Clinical Research Center for Geriatric Disorders, Changsha, People's Republic of China
- <sup>13</sup> Department of Psychiatry, The Second People's Hospital of Hunan Province, The Hospital of Hunan University of Chinese Medicine, Changsha, People's Republic of China
- <sup>14</sup> Department of Neurology, Hunan Aerospace Hospital, Changsha, People's Republic of China
- <sup>15</sup> National Clinical Research Center for Geriatric Disorders, Xiangya Hospital, Central South University, Changsha, People's Republic of China
- <sup>16</sup> Department of Clinical Pharmacology, Xiangya Hospital, Central South University, Changsha, People's Republic of China